Korean J. Chem. Eng., **31**(4), 582-586 (2014)
DOI: 10.1007/s11814-013-0265-7

pISSN: 0256-1115
eISSN: 1975-7220

Characterization and activity of V_2O_5/CeO_2-MgO catalyst in the dehydrogenation of ethylbenzene to styrene

Van-Khoa Nguyen*,, Jung-Hyun Park*, and Chae-Ho Shin*,†**

*Department of Chemical Engineering, Chungbuk National University, Chungbuk 361-763, Korea
**Institute of Chemical Technology, VAST, Vietnam
(*Received 16 January 2013 • accepted 2 December 2013*)

Abstract−Supported vanadia catalyst was impregnated on CeO_2-MgO and characterized by N_2 adsorption, XRD, XPS, TPR and solid NMR. The vanadia species dispersed well on the support surface with vanadia content up to 10 wt%. At higher vanadia content, the non-active $Mg_3(VO_4)_2$ was formed. Vanadium oxides existing on the support surface as tetrahedral vanadium were observed. An ethylbenzene conversion of 43% and styrene selectivity of 91% were obtained with the $10V_2O_5/CeO_2$-MgO catalyst.

Keywords: Ethylbenzene, Dehydrogenation, Vanadia, Ceria, Magnesia

INTRODUCTION

Styrene, one of the most important intermediates in the chemical industry, is commercially produced by the dehydrogenation of ethylbenzene using Fe-K oxide based catalyst in the presence of steam [1,2]. Although commercial catalysts are active, there are some disadvantages such as the unstable oxidation state of active component, low specific surface area, the loss or redistribution of potassium promoters and the physical degradation of the catalyst particles [2,3]. Supported metal oxide catalysts could be used to improve these properties. In previous studies [4-6], the V-Mg-O catalysts were found to be active and selective in the oxidative dehydrogenation of ethane, propane, butane and ethylbenzene. Their catalytic behaviors are related to the formation of Mg-vanadates, the vanadia loadings and/or nature of V^{5+} species on the surface of MgO. Chang [7] found that both the V^{5+} $Mg_3(VO_4)_2$ and the V^{4+} Mg_2VO_4 were active and selective for the oxidative dehydrogenation of ethylbenzene to styrene, while MgV_2O_6 and $Mg_2V_2O_7$ had a low styrene selectivity. The addition of steam into the feed increased the styrene selectivity slightly [7]. The active phase of Mg-vanadates for the oxidative dehydrogenation of propane to propene decreased in the following order: pyro-$Mg_2V_2O_7$>meta-MgV_2O_6>ortho-$Mg_3V_2O_8$ [5,8]. The most active phase was pyro-$Mg_2V_2O_7$ because of the most numerous labile surface lattice oxygen anions. It is shown that the labile surface lattice oxygen anions played an important role in determining the activity of the Mg-vanadates catalyst, and the V-Mg-O catalysts could work well under the steam flowing reaction condition.

Ceria-containing catalyst is used widely in the oxidative reaction because of the two features of CeO_2: the easy redox behavior of Ce^{3+}/Ce^{4+} couple and the high lability of lattice oxygen, properties of which may enhance the activity of vanadia catalyst in the dehydrogenation process. Martinez-Huerta [9] demonstrated that V^{5+}/CeO_2 was active in the oxidative dehydrogenation of ethane. Xu [10] mentioned that the mesostructured CeO_2 could be an effective catalyst for styrene synthesis by oxidative dehydrogenation of ethylbenzene. The previous literature [11] showed that the binary CeO_2-MgO oxide could be used in the catalytic dehydrogenation of ethylbenzene to styrene in the presence of steam. In line with these studies, we synthesized V_2O_5/CeO_2-MgO catalysts with different vanadium oxide content and tried to find the best catalyst of VO_x/CeO_2-MgO for the dehydrogenation of ethylbenzene to styrene. The prepared catalysts were characterized by the BET surface area, X-ray diffraction (XRD), X-ray photoelectron spectroscopy (XPS) and nuclear magnetic resonance (NMR).

EXPERIMENTAL

1. Catalyst Preparation

CeO_2-MgO oxide was prepared by the co-precipitation method as described in previous literature [11]. The mixture of cerium and magnesium with molar ratio of 1 : 9 was dissolved in distilled water and stirred for 30 minutes. The mixed solution was hydrolyzed by the addition of ammonia solution at pH=10. After being aged in the mother liquor at room temperature for 24 h, the precipitate was refluxed at 100 °C for 2 h to get the light yellow solid. The solid was dried at 110 °C for 24 h and then sieved to a mesh size below 210 μm. The final product was calcined at 700 °C for 4 h in the flowing air of 2 *l*/min.

Vanadia was supported on CeO_2-MgO oxide by the impregnation method. Ammonium metavanadate (NH_4VO_3, Aldrich Chemical) was dissolved in oxalic acid solution ($C_2H_2O_4 \cdot 2H_2O$, Shinyo Chemical) with molar ratio of 1 : 3. The concentration of vanadate was adjusted to produce catalysts with V_2O_5 loadings from 3 to 20 wt%. After impregnation, the samples were dried overnight at 110 °C and then calcined at 700 °C for 4 h in the flowing air.

2. Catalyst Characterization

The XRD experiments were performed on a Bruker diffractometer (Model D5005) using CuKα radiation generated at 40 kV and 40 mA. Reference patterns from the International Center for Diffraction Data (ICDD) were used for identification of bulk phases.

†To whom correspondence should be addressed.
E-mail: chshin@chungbuk.ac.kr

The specific surface area, total pore volume and average diameter of the samples were obtained by N_2 sorption at 77 K with a Micromeritics ASAP 2010 analyzer.

The surface vanadium density (VO_X nm^{-2}) was calculated from the following equation: Surface density=$((N_A \times W_V)/(M_V \times S_{BET})) \times 10^{-18}$, in which, N_A is Avogadro's constant, W_V the mass fraction of vanadium in catalysts (wt%), M_V the molecular weight of vanadium (50.94 g mol^{-1})and S_{BET} the specific surface area of catalysts (m^2 g^{-1}).

The temperature programmed reduction was performed on a Micromeritics Autochemi II 2920 instrument. Prior to TPR studies, the catalyst sample was pretreated at 400 °C for 3 h in flowing helium to eliminate the moisture. After being pretreated, the sample was cooled to room temperature, then heated at a rate of 10 °Cmin^{-1} to 900 °C under the flow of reducing gas. The reducing gas was a mixture of 10 vol% H_2 in air and its flow rate was 50 cm^3min^{-1}. The amount of H_2 consumed by catalyst sample in a given temperature range was determined by TCD detector.

XPS measurements were performed in a VG ESCALAB 210 model equipped with an MgK_α (1,253.6 eV) source. The binding energy scale was calibrated to Au $4f_{7/2}$ line of 83.95 eV. Referencing the adventitious Si 2p peak set at 103.6 eV was used for charge compensation. Each data set was first corrected for the non-linear emission background. The data was then fitted with Gaussian function to find the peak position.

Magic angle spinning (MAS) ^{51}V NMR spectra were recorded at 105.2 MHz on a Bruker AVANCE 500 spectrometer equipped with an MAS probe for 4 mm outer diameter rotors. Rotation frequencies of 10-12 kHz were used. In all experiments, a single pulsed excitation of 1.5 μs was applied. The dead time and the recycle time was 10 μs and 5 s, respectively.

3. Reaction Conditions

The catalytic activity was determined, based on the dehydrogenation of ethylbenzene to styrene. This process was carried out at 600 °C in continuous flow micro-reactor system at atmospheric pressure. Prior to the activity measurement, the catalyst was activated in the steam flow of 50 ml/min by heating up to 650 °C at the rate of 2.5 °C/min. After remaining at 650 °C for 2 h, the reaction temperature was decreased to 600 °C. Water (partial pressure of 76.4 torr) and ethylbenzene (partial pressure of 8.4 torr) in helium, a balancing gas (GHSV=80,000 h^{-1}), were fed into a quartz reactor containing of 0.15 g of catalyst. All products of the ethylbenzene dehydrogenation such as styrene, benzene, toluene and ethylbenzene were analyzed by gas chromatography (Chrompack-CP9001) equipped with flame ionization detector and capillary CP Chirasil-Dex CB DF=0.25. Total conversion of ethylbenzene is defined as the percentage of ethylbenzene converted to hydrocarbon products, while styrene selectivity is supposed to be the percentage of styrene in the observed product.

RESULTS AND DISCUSSION

1. Characterization of Catalyst

The textural parameters of the supported vanadium oxide catalysts are given in Table 1. The BET surface area decreased with the increase of V_2O_5 loading. There are usually two reasons for the decrease of surface area of supported catalysts: first, some pores are blocked by the supported species, and second, solid reaction may occur between the support and supported species to form some new compounds [12]. Actually, the XRD pattern of V_2O_5/CeO_2-MgO catalysts with different vanadia loadings showed that the $Mg_3(VO_4)_2$ phase had been formed at high vanadia loadings (Fig. 1).

Table 1. Textural properties of CeO_2-MgO supported vanadium oxide catalysts

Catalysts	S_{BET} (m^2 g^{-1})	Pore volume (cm^3 g^{-1})	Surface density (nm^{-2})[a]
CeO_2-MgO	43	0.272	
$3V_2O_5/CeO_2$-MgO	36	0.241	5.52
$5V_2O_5/CeO_2$-MgO	29	0.211	11.42
$10V_2O_5/CeO_2$-MgO	26	0.166	25.47
$15V_2O_5/CeO_2$-MgO	26	0.166	38.20
$20V_2O_5/CeO_2$-MgO	24	0.156	55.18

[a]Calculated from Ref. 31

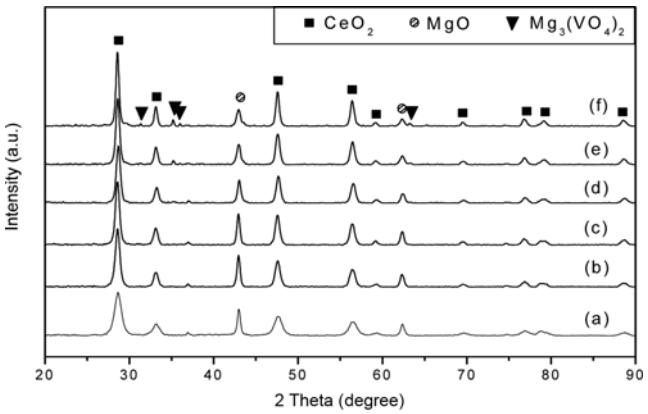

Fig. 1. XRD patterns of the V_2O_5/CeO_2-MgO catalysts; (a) CeO_2-MgO, (b) $3V_2O_5$, (c) $5V_2O_5$, (d) $10V_2O_5$, (e) $15V_2O_5$ and (f) $20V_2O_5$.

For vanadia loadings up to 10 wt%, only the characteristic peaks of ceria and magnesia phase were observed. The ceria peaks were located on 28.5°, 33.0°, 47.5° and 56.4° [JCPDS 43-1002] and the MgO peaks were centered at 37.0°, 42.8° and 62.2° in 2θ [JCPDS 43-1022]. There were no vanadate peaks for the catalysts with the vanadia loadings from 3 to 10 wt% since vanadium oxide had dispersed well on the support surface. However, with the vanadia loading of higher than 10 wt%, new characteristic peaks of $Mg_3(VO_4)_2$ emerged at 31.5°, 35.3°, 36.0°, 43.8° and 63.6° in 2θ [JCPDS 37-0351]. That is due to the reaction between sintered vanadia and free MgO forming $Mg_3(VO_4)_2$ on the supported surface. This result suggested that the vanadia loading of 10 wt% was the limiting content of vanadia for monolayer dispersion. In the studies [9,12-14], vanadia dispersed well on CeO_2 with low vanadia loadings. The monolayer dispersion capacity was found to be 10 wt% of V_2O_5, while the higher loadings resulted in the formation of $CeVO_4$. However, in our sample, the $CeVO_4$ phase could not be detected with any vanadia loadings. Because magnesia content is so much larger than that of ceria, all of ceria reacted to magnesia forming binary CeO_2-MgO oxide [11]. The simultaneous existence of free MgO phase and Ce-Mg-O phase in the CeO_2-MgO support was demonstrated previ-

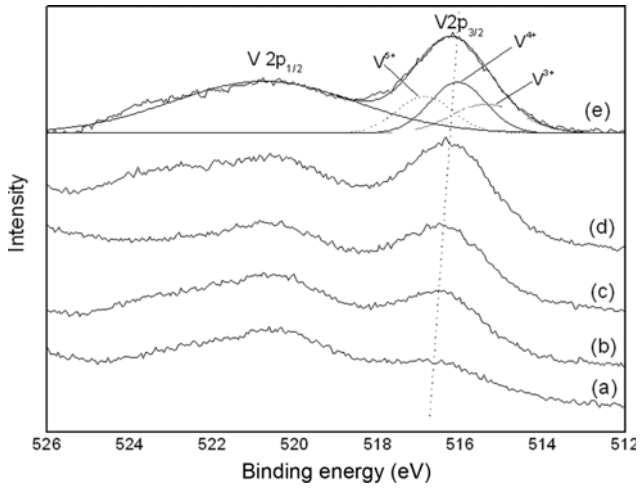

Fig. 2. XPS of V 2p of V_2O_5/CeO_2-MgO catalysts; (a) $3V_2O_5$, (b) $5V_2O_5$, (c) $10V_2O_5$, (d) $15V_2O_5$ and (e) $20V_2O_5$.

ously [11]. For this reason, the bond of vanadia and magnesia was formed without V-Ce bond even with the high vanadia content impregnated on CeO_2-MgO support surface.

The XPS of vanadium on V_2O_5/CeO_2-MgO catalyst is given in Fig. 2. The broad features centered at 516.2 eV correspond to the V $2p_{1/2}$ state. A satellite peak around 520.5 eV, which was associated with V^{5+}, was also observed in all XPS [16]. The binding energy shifted to higher value with the increase of vanadia content. The broad peak suggested that the deposited vanadium had multi oxidation states. The deconvolution of the V $2p_{3/2}$ peak based on a Gaussian signal showed three peaks located on 515.4, 516.1 and 516.9 eV corresponding to V^{3+}, V^{4+} and V^{5+}, respectively. These peak positions are similar to those reported in previous studies [14-17], in which the binding energy of V $2p_{3/2}$ for V^{3+}, V^{4+} and V^{5+} was located around 515.5-515.9, 516-516.5 and 516.8-517.7 eV, respectively.

^{51}V MAS NMR spectra of the CeO_2-MgO supported vanadium oxide catalysts are obtained at static shown in Fig. 3. There is only one peak at −557 ppm corresponding to the tetrahedral vanadia species. The broadness of the peak suggests a distorted environment

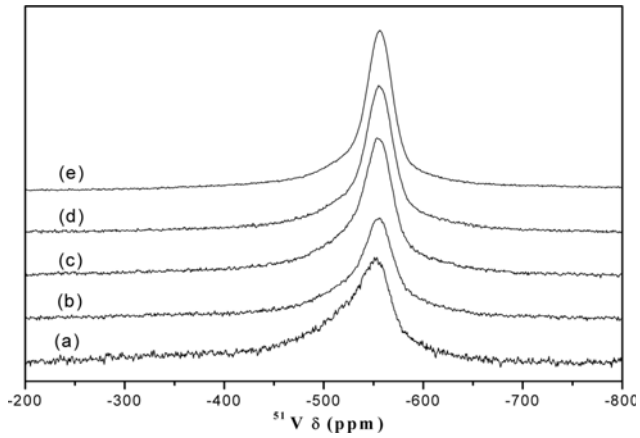

Fig. 3. ^{51}V MAS NMR spectra of V_2O_5/CeO_2-MgO catalyst: (a) $3V_2O_5$, (b) $5V_2O_5$, (c) $10V_2O_5$, (d) $15V_2O_5$ and (e) $20V_2O_5$ (at static).

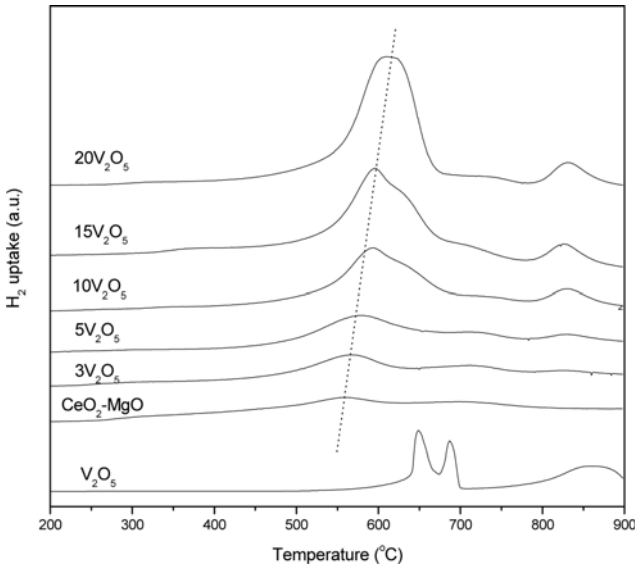

Fig. 4. TPR profiles of V_2O_5/CeO_2-MgO catalysts: (a) CeO_2-MgO, (b) $3V_2O_5$, (c) $5V_2O_5$, (d) $10V_2O_5$, (e) $15V_2O_5$, (f) $20V_2O_5$ and the profile marked by dashed line describes the reduction of bulk V_2O_5.

of oxygen atoms around tetrahedral vanadia species. This result agrees with ^{51}V NMR in the previous literature [14-17]. The band of the tetrahedral V^{5+} species was located around −550 ppm together with the vanadia catalyst on the various supports such as MgO, Mg-Al hydrotalcite, sepiolite, Al_2O_3-TiO_2 and Al_2O_3 [18-21].

The TPR profiles of bulk vanadium oxide and various V_2O_5/CeO_2-MgO catalysts are shown in Fig. 4. The TPR profile of bulk V_2O_5 including three peaks was ascribed to reduction in different steps: $V_2O_5 \rightarrow V_6O_{13} \rightarrow V_2O_4 \rightarrow V_2O_3$ [22,23]. The reduction of bulk V_2O_5 is carried out at higher temperature in comparison to the reduction of supported vanadium oxide catalysts. This is supposed to be due to the increased diffusion limitation in bulk V_2O_5 [24]. The TPR profile of the CeO_2-MgO support exhibited two peaks at 553 and 688 °C. The peak at the low temperature corresponds to the reduction of surface of the Ce^{4+} to the Ce^{3+}, and the peak at high temperature peak is assigned to reduction of bulk CeO_2 [12].

As we know, the vanadium oxide in very low concentration could form isolated vanadium oxide VO_x species. The molecular structures of these surface vanadia species are tentatively thought to consist of a terminal V=O bond and three bridging V-O-support bonds for the isolated species. At higher concentrations, still below the theoretical monolayer capacity, a two-dimensional surface phase is known to develop. A terminal V=O bond with one bridging V-O-support and two bridging V-O-V bonds is for the polymerized species. A disordered or a paracrystalline V_2O_5 phase exists at the concentrations over the monolayer point [25-27]. In our sample, with the vanadia loading from 3 to 5 wt% (below the monolayer concentration capacity), there were two reduction peaks at 567-577 °C and 825-831 °C corresponding to the release of oxygen of the V-O-support and a terminal V=O bond, respectively [26,27]. With increasing surface vanadium oxide loading from 10 to 20 wt%, the vanadium oxide species will agglomerate forming polymeric chains of tetrahedral VO_4 species. In this case, the reduction of vanadium oxide species, which is similar to bulk V_2O_5, had three peaks. The

new shoulder peak located around 630-640 ℃ reflects the contribution of the release of the oxygen of the bridging V-O-V bond in polyvanadate species. It is easily seen from the figure that the $T_{one\text{-}set}$ peak shifted to higher temperature level since the polyvanadate species formed with increasing vanadia content, which possessed a likely bulk vanadia structure. The change of reduction temperature could affect the selectivity and activity of ethylbenzene dehydrogenation.

2. Activity of Catalysts

Fig. 5(a) shows that the ethylbenzene conversion increased from 35 to 43% and the styrene selectivity increased from 85 to 91% with vanadia loading from 3 to 10 wt%. At the vanadia loading over 10 wt%, the ethylbenzene conversion was not stable and decreased progressively with time on stream, while the styrene selectivity increased slightly.

The XRD pattern shows that vanadia of 10 wt% was determined as the monolayer dispersion content capacity. So, the ethylbenzene conversion and the styrene selectivity increased with vanadia loadings up to 10 wt%. The $Mg_3(VO_4)_2$ phase was formed with the vanadia loading over monolayer concentration capacity. This is the reason for the reduction of the catalytic activity with the vanadia loadings over 10 wt%. However, the $Mg_3(VO_4)_2$ phase had a small enhancement of the styrene selectivity in the oxidative dehydrogenation of ethylbenzene [7]. This property may help to explain the slight increase of styrene selectivity with higher vanadia content. The result suggests that the $Mg_3(VO_4)_2$ phase is non-active for the dehydrogenation of ethylbenzene, although it is opposite to the report of Chang [7], which demonstrated that the $Mg_3(VO_4)_2$ phase was active in the oxydehydrogenation of ethylbenzene. Furthermore, some authors [27-29] suggested that the reducibility of vanadates determines the selectivity to the oxydehydrogenation reaction of short alkanes. It indicates that the more reducible the catalyst is, the less selective it is. Fig. 4 shows that the reduction temperature shifted to higher level with increasing vanadia loadings. It means that the reducibility of the surface vanadia catalyst is difficult to occur at high vanadia loadings. Therefore, the catalyst selectivity increases with increasing vanadia loadings. As discussed above, the temperature of reduction shifted to higher level because of the formation of dimeric and/or polymeric vanadate species which possessed the structure containing the V-O-V bond. In the study of Wegrzyn [30], oxygen atom in V-O-Mg bond is demonstrated to be more nucleophilic (basic) than that in V-O-V bond. The nucleophilic oxygen anions activate hydrocarbon molecule by hydrogen abstraction leading to dehydrogenation. Electrophilic (acidic) oxygen anions in V-O-V bond lead to total oxidation. For our sample, the V-O-support bond was formed predominantly at low vanadia content. Thus, the dehydrogenation may proceed. At higher vanadia content, the formation of V-O-V bond was enhanced, hence, the oxidation reaction was enhanced leading to the decrease of the styrene selectivity, and it easily made coking on the catalyst surface, leading to the decrease of catalyst activity.

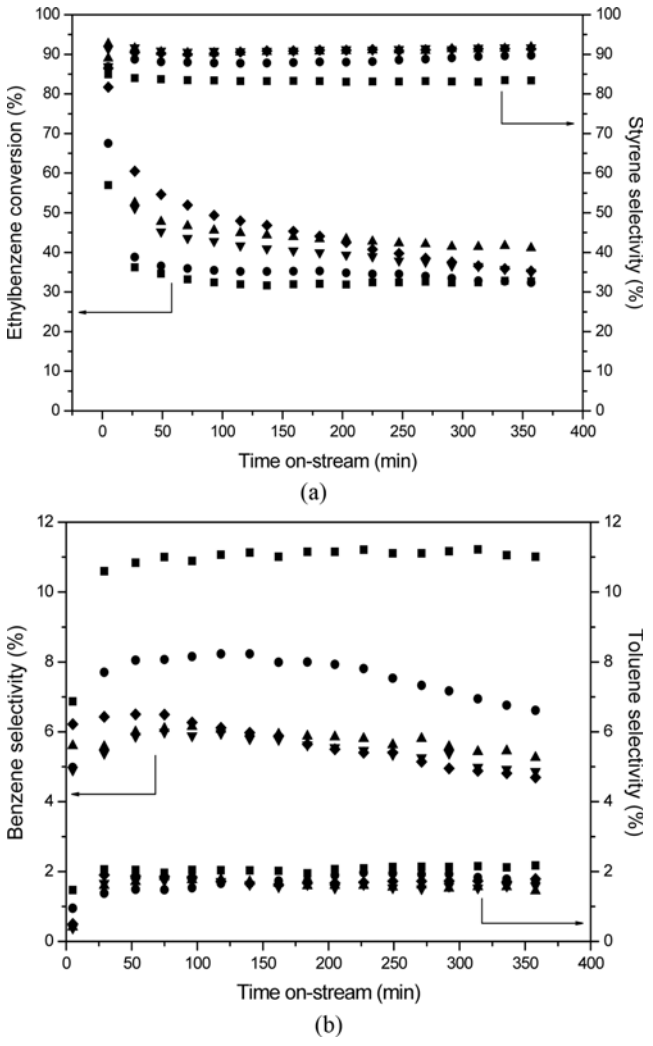

Fig. 5. (a) and (b): Catalytic activity of V_2O_5/CeO_2-MgO catalysts with different vanadia content: $3V_2O_5$ (■); $5V_2O_5$ (●); $10V_2O_5$ (▲); $15V_2O_5$ (▼) and $20V_2O_5$ (◆) versus time on stream.

The formation of the by-products, benzene and toluene, in the dehydrogenation process is given in Fig. 5(b). The result shows that the yield of benzene is much higher than that of toluene. The formation of benzene and styrene decreased with increasing vanadia loading from 3 to 10 wt%, while the by-products were almost unchanged with the further increase of vanadia loading.

CONCLUSIONS

The V_2O_5/CeO_2-MgO catalyst was active and selective for ethylbenzene dehydrogenation in the presence of steam. The ethylbenzene conversion depends on the vanadia dispersion, while the styrene selectivity depends on the reducibility of vanadia catalyst. Vanadia content 10 wt% was determined as the monolayer dispersion capacity. The ethylbenzene conversion increased from 35 to 43% and the styrene selectivity increased from 85 to 91% with vanadia loading from 3 to 10 wt%. At the vanadia loading over 10 wt%, the ethylbenzene conversion was not stable and decreased progressively with time on stream, while the styrene selectivity increased slightly. The catalytic activity with the ethylbenzene conversion of 43% and the styrene selectivity of 91% were obtained with the 10 V_2O_5/CeO_2-MgO catalyst.

ACKNOWLEDGEMENTS

This work was financially supported by the grant from the Indus-

trial Source Technology Development Programs (2013-10042591) of the Ministry of Trade, Industry & Energy (MOTIE) of Korea and partially by the research grant of Chungbuk National University in 2012.

REFERENCES

1. F. Cavani and F. Trifiro, *Appl. Catal. A*, **133**, 219 (1995).
2. A. Kotarba, W. Bieniasz, P. Kustrowski, K. Stadnicka and Z. Sojka, *Appl. Catal. A*, **407**, 100 (2011).
3. A. C. Oliveira, J. L. G. Fierro, A. Valentini, P. S. S. Nobre and M. C. Rangel, *Catal. Today*, **85**, 49 (2003).
4. B. Y. Jibril, A. Y. Atta, K. Melghit, Z. M. El-Hadi, A. H. Al-Muhtaseb, *Chem. Eng. J.*, **193-194**, 391 (2012).
5. Y. Takita, Q. Xia, K. Kikutani, K. Soda, H. Takami, H. Nishiguchi and K. Nagaoka, *J. Mol. Catal. A*, **248**, 61 (2006).
6. D. Y. Hong, V. P. Vislovskiy, Y. K. Hwang, S. H. Jhung and J. S. Chang, *Catal. Today*, **131**, 140 (2008).
7. W. S. Chang, Y. Z. Chen and B. L. Yang, *Appl. Catal. A*, **124**, 221 (1995).
8. A. Guerrero-Ruiz, I. Rodriguez-Ramos, J. L. G. Fierro, V. Soenen, J. M. Herrmann and J. C. Volta, *Stud. Surf. Sci. Catal.*, **72**, 203 (1992).
9. M. V. Martinez-Huerta, J. M. Coronado, M. Fernandez-Garcia, A. Iglesias-Juez, G. Deo, J. L. G. Fierro and M. A. Banares, *J. Catal.*, **225**, 240 (2004).
10. J. Xu, L. C. Wang, Y. M. Liu, Y. Cao, H. Y. He and K. N. Fan, *Catal. Lett.*, **133**, 307 (2009).
11. V. K. Nguyen, J. H. Park and C. H. Shin, *Reac. Kinet. Mech. Cat.*, **107**, 157 (2012).
12. X. Gu, J. Ge, H. Zhang, A. Auroux and J. Shen, *Thermochim. Acta*, **451**, 84 (2006).
13. H. L. Abbott, A. Uhl, M. Baron, Y. Lei, R. J. Meyer, D. J. Stacchiola, O. Bondarchuk, S. Shaikhutdinov and H. J. Freund, *J. Catal.*, **272**, 82 (2010).
14. A. M. Duarte de Farias, P. Bargiela, M. G. C. Rocha and M. A. Fraga, *J. Catal.*, **260**, 93 (2008).
15. C. Hess and R. Schogl, *Chem. Phys. Lett.*, **432**, 139 (2006).
16. J. M. Vohs, T. Feng and G. S. Wong, *Catal. Today*, **85**, 303 (2003).
17. G. S. Wong and J. M. Vohs, *Surf. Sci.*, **498**, 266 (2002).
18. T. Blasco and J. M. Lopez Nieto, *Colloids Surf., A*, **115**, 187 (1996).
19. H. J. Chae, I. S. Nam, S. W. Ham and S. B. Hong, *Appl. Catal. B*, **53**, 117 (2004).
20. J. M. Miller and L. J. Lakshmi, *J. Mol. Catal. A*, **144**, 451 (1999).
21. E. F. Aboelfetoh, M. Fechtelkord and R. Pietschnig, *J. Mol. Catal. A*, **318**, 51 (2010).
22. M. Koranne, J. G. Goodwin and G. Marcelin, *J. Catal.*, **148**, 369 (1994).
23. H. Zhao, S. Bennici, J. Cai, J. Shen and A. Auroux, *J. Catal.*, **274**, 259 (2010).
24. E. P. Reddy and R. S. Varma, *J. Catal.*, **221**, 93 (2004).
25. B. M. Reddy, K. N. Rao, G. K. Reddy and P. Bharali, *J. Mol. Catal. A*, **253**, 44 (2006).
26. N. R. Shiju, M. Anilkumar, S. P. Mirajkar, C. S. Gopinath, B. S. Rao and C. V. Satyanarayana, *J. Catal.*, **230**, 484 (2005).
27. F. Klose, T. Wolff, H. Lorenz, A. Seidel-Morgenstern, Y. Suchorski, M. Piorkowska and H. Weiss, *J. Catal.*, **247**, 176 (2007).
28. T. Blasco and J. M. Lopez Nieto, *Appl. Catal. A*, **157**, 117 (1997).
29. F. Tang, K. Zhuang, F. Yang, L. Yang, B. Xu, J. Qiu and Y. Fan, *Chinese J. Catal.*, **33**, 933 (2012).
30. A. Wegrzyn, A. Rafalska-Lasocha, B. Dudek and R. Dziembaj, *Catal. Today*, **116**, 74 (2006).
31. M. Setnicka, R. Bulanek, L. Capek and P. Cicmanec, *J. Mol. Catal. A*, **344**, 1 (2011).